Vanadium Oxide Oligomers and Ordered Monolayers Supported on CeO_2(111): Structure and Stability Studied by Density Functional Theory

Christopher Penschke,[†] Joachim Paier, and Joachim Sauer*

Institut für Chemie, Humboldt-Universität zu Berlin, Unter den Linden 6, 10099 Berlin, Germany

ABSTRACT: Structures and stabilities of vanadium oxide oligomers as well as two candidate structures for a monolayer on the CeO_2(111) surface have been studied by density functional theory employing a genetic algorithm to determine the global energy minimum structures. These ceria-supported structures have predominantly four-fold coordinated V^{5+} ions with V=O groups in common. The agglomeration of VO_2 clusters deposited on the surface is a strongly exothermic process, particularly when ring structures with three or six VO_2 units are formed that are commensurate with the close-packed surface-terminating oxygen layer. The VO_2 and V_2O_5 monolayers feature larger coordination numbers (5, 6) of V and contain V atoms without V=O groups. Relative to oligomers, VO_2 and V_2O_5 monolayer structures with and without oxygen defects are thermodynamically more stable. This, together with the fact that flat "monolayer" clusters are preferred to taller "bilayer" clusters, indicates the preference for a complete 2D wetting of the ceria support.

1. Introduction

Vanadium oxides, or vanadia for short, supported on other metal oxides are important components of active as well as selective solid catalysts applied in many industrially relevant oxidation reactions.[1-3] The oxidative dehydrogenation (ODH) of low alcohols such as methanol[4-10] or ethanol[11-13] on oxide supported vanadia is an intensely studied reaction in the context of C–H bond activation. It was shown that vanadia supported on reducible oxides like ceria or titania is, in terms of turnover frequency, three to four orders of magnitude more active than vanadia on non-reducible supports like SiO_2.[4-7] Similar observations have been made for the ODH of propane.[14] Preparation conditions and support affect type and distribution of the vanadia species, which is likely the reason for the variation in turnover frequencies with the support for given vanadium loadings.[14-16] Depositing vanadia on oxides which are themselves dispersed on a different support may also strongly affect the reactivity, as shown, e.g., by Bañares and coworkers for a ternary $VO_x/CeO_2/SiO_2$ system.[17]

The activity in selectively oxidizing methanol to formaldehyde at ceria-supported vanadia catalysts depends on the amount of vanadium deposited on the surface.[9,18-19] To understand this behavior at the atomic level, model studies are indispensable.[20] The reactivity of vanadia on well-defined $CeO_2(111)$ model systems was shown to be comparable to that of powder catalysts,[11,18] suggesting that the models capture essential features of the supported vanadia species. Scanning tunneling microscopy (STM) images of VO_x deposited on well-defined $CeO_2(111)$ films showed a wide distribution of isolated, two-dimensional vanadia species.[21] Upon increasing vanadia coverage and upon annealing, monomers agglomerate to form larger species, in particular trimers and heptamers. The same study reported X-ray photoelectron spectroscopy (XPS) results indicating that vanadium is accommodating its highest oxidation state +5, while Ce^{4+} ions of the support are reduced to Ce^{3+}. Combining temperature-programmed desorption (TPD) and STM revealed that the monomers are more active in the ODH of methanol than trimers and larger oligomers.[19]

Ceria-supported vanadia MLs have been extensively studied experimentally for powder catalysts, but detailed atomistic information has not become available yet.[9,18,22-23] The complete ML represents an important limiting case in terms of activity. Beyond ML coverage, V_2O_5 crystallites are formed, which have a much lower active site density than VO_x supported on $CeO_2(111)$.[6] Furthermore, the variation in activity with the support indicates that the V-O-M (M = support metal cation) interphase bond plays an important role.[8,24-26] Different values for the vanadium content of the ML were obtained by different groups. Burcham and Wachs reported 5.7 V atoms/nm^2 corresponding to the highest loading for which no Raman bands typical of V_2O_5 crystallites were observed.[23] On the other hand, Feng and Vohs performed TPD experiments after exposing the (powder) catalyst to methanol.[9] They reported that the high-temperature CO desorption peak at ca. 615 K, characteristic for methanol oxidation on the employed pure ceria, does not appear for vanadia loadings higher than 9.5 V atoms/nm^2. According to these authors, this indicates exhaustive (2D) coverage of the ceria surface and thus formation of a complete ML.

The oxygen content of the ML, i.e. whether it corresponds to a fully oxidized V_2O_5 layer or to a layer with the composition of a reduced vanadium oxide phase like V_2O_3, is not directly accessible by experiment. As mentioned above, this is because vanadium is readily oxidized to V^{5+} by ceria.[21] In refs. 19,21,24 and 27, physical vapor deposition was employed to deposit vanadia on the $CeO_2(111)$ films, while the work by Feng and Vohs[9] was accomplished for samples prepared via incipient wetness impregnation. According to their XPS results, nonreduced (so-called stoichiometric) CeO_2 was present, i.e. no reduction to Ce^{3+} upon vanadia deposition was observed. This indicates that the (electronic) structure of the vanadia ML catalyst may depend on the actual preparation technique.

Density functional theory (DFT) calculations on small vanadia clusters (up to trimers) on $CeO_2(111)$ were compatible with the experimental results, in particular the stabilization of V^{5+} by reduction of Ce^{4+} to Ce^{3+} ions[21,28-29] and the thermodynamic preference of VO_2 trimers[29]

compared to kinetically stabilized[30] monomers. Furthermore, detailed mechanistic DFT studies on the rate-determining hydrogen abstraction[31-32] reported lower barriers for supported monomers[33] compared to trimers,[34] in agreement with experimental results.

Recently, Gong and coworkers argued that they have found a more stable structure for the VO_2 monomer on $CeO_2(111)$.[35-36] However, their structure is *de facto* identical with the one reported previously by this group.[19,28-30,33] Therefore, contrary to the statements made in refs. 35 and 36, our previous calculations do refer to the most stable structure of ceria-supported VO_2.

The present work employs DFT for examining structures and stabilities of 2D vanadium oxides on the $CeO_2(111)$ surface for intermediate coverages as well as for the important limiting case of a complete ML. The latter is particular relevant because no support surface is exposed and there are no vanadia ad-particle/ceria surface edges present. The reaction will happen on a vanadia film whose geometric structure is given by the supporting (cerium) oxide underneath and whose electronic structure is modified by the vanadia/ceria interphase.

The supported vanadia oligomers were built from VO_2 units, as comparison of earlier work in our group[22,23] with experimental results[21] revealed them to be more likely candidates than species with different vanadium-oxygen ratios. In particular, we found that (i) trimerization of VO_2 monomers on $CeO_2(111)$ is strongly exothermic, in contrast to supported VO;[29] (ii) supported VO_2 features terminal V=O bonds, in contrast to supported VO_4 clusters;[28] and (iii) Ce^{3+} ions are created by electron transfer from supported VO_2, in contrast to supported VO_3 and VO_4 clusters.[28] The last point also suggests that V_2O_5 clusters are unlikely to be the relevant species, at least under the ultra-high vacuum conditions used in ref. 21. However, due to the stability of V_2O_5 in bulk phase, we performed calculations on a supported V_2O_5 cluster (shown in the Supporting Information). It is less stable than supported VO_2 clusters in the range of conditions considered in this work. Therefore, we decided to focus on clusters with VO_2 composition.

Two approaches to construct models of supported vanadium oxide ML structures are reported in the literature: (i) substitution of metal atoms of the support with vanadium atoms, for example in anatase TiO_2(001),[37] α-Al_2O_3(0001),[38] κ-Al_2O_3(001)[39] and Al_2O_3/NiAl(110),[40] or (ii) deposition of vanadium oxide layers cut from bulk phases on the support, e.g. V_2O_3 on Al_2O_3/NiAl(110)[40] and V_2O_5 on anatase TiO_2(001).[37,41-42] Thus, the monolayers are typically structurally similar either to the support or the corresponding bulk vanadium oxide. This is different with monolayers on CeO_2(111). The hexagonal surface structure prevents direct deposition of V_2O_5(001) layers due to the strong crystallographic mismatch. Creation of an interface between CeO_2(111) and V_2O_3(0001) is hampered by a large lattice mismatch of ca. 25% between the calculated surface lattice parameters of 388 and 486 pm, respectively.[43-44] As a consequence, ceria-supported monolayers will be structurally rather different from most of the monolayers on other supports.

To sample the potential energy surface of a given composition, a genetic algorithm (GA) is used to determine global energy minimum structures. Specifically, the "DoDo" algorithm is used, which was developed in-house and has been successfully applied to solve the structure of ordered water monolayers on the MgO(001) surface.[45]

For the energy minimum structures found for the different supported vanadia aggregates we discuss relative stabilities and report energies required to create oxygen point defects in the various structures, which characterize their reducibilities. We summarize these results as a stability diagram. In addition, harmonic wavenumbers of V=O stretch vibrations are presented.

2. Models and methods

2.1. Surface model. The surface model was created by cutting the CeO_2 unit cell of the bulk phase (employing an optimized lattice constant of 549 pm)[43] along the (111) plane. Results reported in this work use a $p(4 \times 4)$ surface unit cell. The slab model consists of 9 atomic layers,

resulting in a composition of $Ce_{48}O_{96}$. We use asymmetric slab models, i.e. positions of atoms residing in the bottommost O-Ce-O tri-layer were fixed to preserve the geometric structure as in the bulk phase. The Brillouin zone was sampled for integration using only the zone center Γ. The employed vacuum layer was set to 10 Å.

As mentioned in the introduction, the literature values for a complete ML on CeO_2(111) range from 5.7 V atoms/nm^2 (ref. 23) up to 9.5 V atoms/nm^2 (ref. 9). These two numbers correspond to approximately 0.75 and 1.25 V atoms per surface Ce atom. This work uses the corresponding mean value, i.e. 1 V atom per surface Ce atom, to define the ML coverage. This value is identical to a coverage of 8 V atoms/nm^2, as suggested by Burcham and Wachs for the average vanadia content of a ML supported on various metal oxides.[23] Since the $p(4 \times 4)$ surface unit cell contains 16 Ce atoms in each cation layer, a single vanadium atom is equivalent to $^1/_{16}$ or 6.25 % of a ML.

2.2. Electronic and ionic structure optimizations. Calculations were performed using the projector augmented wave method (PAW)[46-47] to describe the interaction between ionic cores and valence electrons as implemented in the Vienna *ab initio* simulation package (VASP).[48-49] The PAW potentials comprise 12 ([Xe] $5s^2 5p^6 4f^1 5d^1 6s^2$), 6 ([He] $2s^2 2p^4$) and 11 ([Mg] $3p^6 4s^2 3d^3$) valence electrons for Ce, O and V, respectively. For Ce, the cutoff radii for the partial waves are 1.5 and 1.65 au for 5s and 6s, 1.8 for 5p, 2.3 for 5d and 2.57 au for 4f. The cutoff radii for the partial waves employed for O are 1.2 and 1.52 au for 2s and 2p orbitals and 2.0, 2.3 and 2.3 au for 3p, 4s and 3d orbitals of V, respectively. The onsite Coulomb correlation of occupied Ce 4*f* orbitals is corrected via the DFT+U approach[50-51] employing the gradient-corrected exchange-correlation functional by Perdew, Burke, and Ernzerhof (PBE)[52] and an *effective* Hubbard-type U parameter of 4.5 eV. The specific implementation of DFT+U used in this work follows Dudarev *et al*.[53-54]

A plane wave kinetic energy cutoff of 600 eV was used and structure optimizations were performed until forces acting on the relaxed atoms were below 0.02 eV $Å^{-1}$. Starting from these minima, the structures were reoptimized with the DFT-D2 dispersion correction scheme by Grimme.[55] A cutoff radius for the pair interactions has been used,[56] but as discussed in ref. 29, employing the Ewald summation technique[57] gives virtually identical results. For C_6 and R_0 parameters of Ce, see ref. 29.

Orbitally projected densities of states (DOS) and local magnetic moments of Ce (or V) species are obtained by projecting the crystal orbitals into spherical harmonics of f (or d) symmetry located in atom centered PAW spheres with a radius of 1.323 (or 1.217) Å. A typical value of local magnetic moments for Ce^{3+} is $\pm 0.96\ \mu_B$ for up (+) and down spin (–), respectively.

For the local optimization within the genetic "DoDo" algorithm, a smaller plane wave kinetic energy cutoff of 300 eV as well as the so-called soft oxygen pseudopotential have been applied. Starting from the VO_2-tetramer, the most stable structures of smaller species have been introduced into the initial population as so-called seeds. This procedure speeds up convergence of the evolutionary search, but it may also introduce a bias towards certain structures. However, we try to overcome this problem by using additional random structures in the initial population and maintaining a large and structurally diverse population.

Molecular dynamics (MD) simulations were performed on the ML structures to refine the structures obtained using the GA and the manually generated structures. A Nosé thermostat employing a temperature of 1000 K and a time step of 1 fs has been used.

Vibrational frequencies and normal modes were obtained by diagonalizing a partial, mass-weighted matrix of second derivatives of the energy with respect to the three Cartesian degrees of freedom of each adatom. This 'Hessian' matrix was obtained by finite-differences of the gradients with displacements of ±0.015 Å (central differences). Relative intensities were calculated based on the dipole moment change perpendicular to the surface.[58]

3. Results and Discussion

3.1. Vanadia oligomers on CeO_2(111). The lowest-energy structures for various adsorbed clusters built from VO_2 units are shown in Figure 1. The monomer and trimer structures are not included, because they are identical to those published earlier.[29] However, a new dimer structure was found which is 0.30 eV/V atom more stable than the structure shown in Figure 1 of ref. 29. This is due to the different coordination environment in vicinity of the cluster. In the previous structure, binding of the cluster to surface oxygen atoms results in two 6-fold coordinated Ce ions (i.e., they lost one coordination compared with Ce in the regular surface), while in the new structure, 7-fold coordination for one of them is restored by an oxygen atom from the cluster.

In agreement with results obtained for small oligomers, the support stabilizes V in the +5 oxidation state and the VO_4 tetrahedron is the predominant building block. Structures with reduced vanadium ions or smaller coordination numbers for V than four are significantly less stable. Larger coordination numbers were found in a few structures, specifically in the V_8O_{16} structure, which contains two 5-fold coordinated vanadium ions (V_{5c}). V-O bond distances are reported in Table 1.

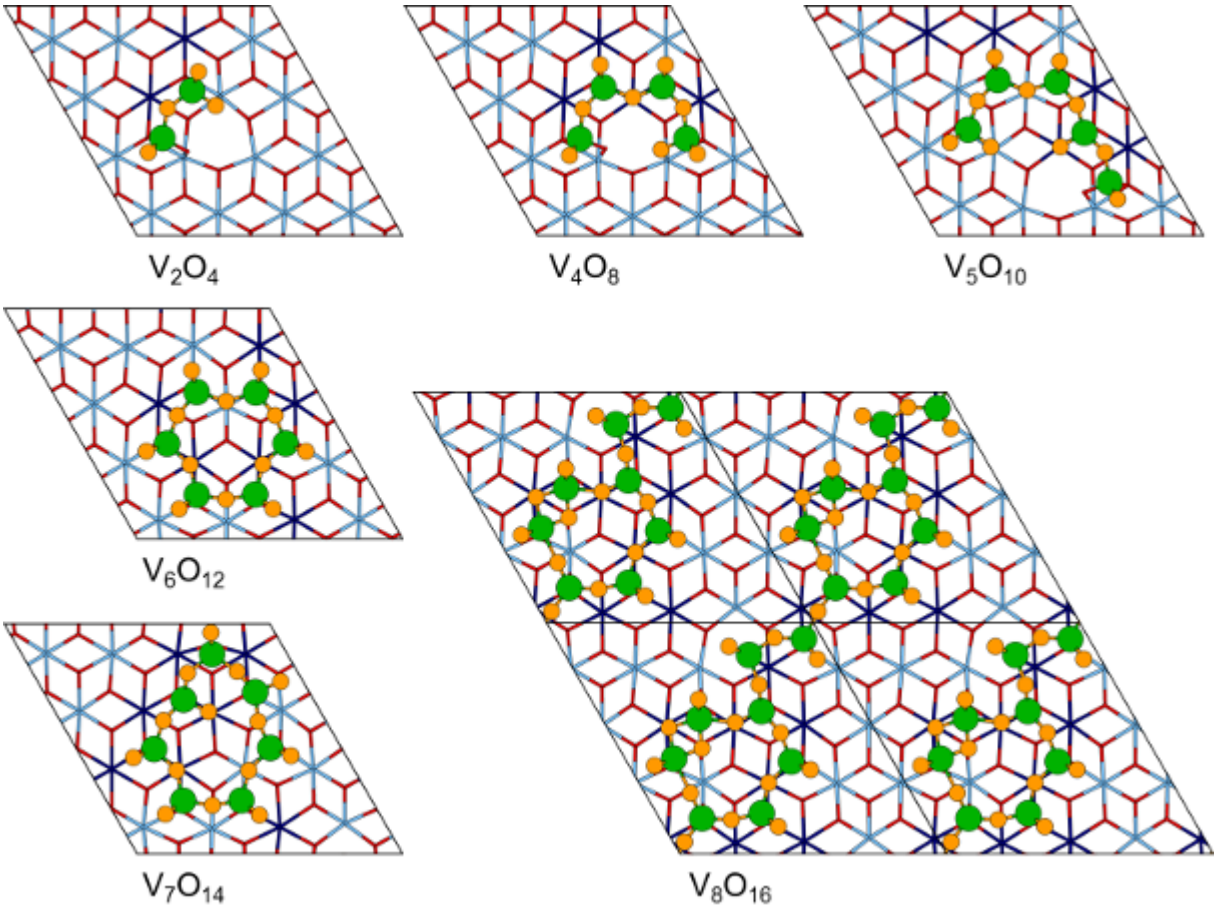

Figure 1. Most stable $V_nO_{2n}/CeO_2(111)$ (n = 2, 4 – 8) structures. For clarity, only the topmost O-Ce-O trilayer is shown. Ce^{4+} and Ce^{3+} cations are shown in light and dark blue, respectively. Vanadium and oxygen atoms of the adsorbed cluster are depicted in green and orange, respectively, while oxygen atoms of the ceria surface are shown in red. Four unit cells of $V_8O_{16}/CeO_2(111)$ are shown to highlight its extended structure. All pictures were generated using the XCrysDen program.[59]

For a given composition, the most stable structure contains the oligomer of highest nuclearity instead of 'fragments', i.e. isolated smaller oligomers. For instance, the V_6O_{12} structure shown in Figure 1 is 0.29 eV more stable than two separate V_3O_6-rings at the same coverage. Except for the V_8O_{16} structure, linkage of oligomers across cell boundaries to form extended structures did not occur or was unfavorable in terms of stability. Furthermore, formation of two-dimensional clusters is preferred over three-dimensional growth.

Oligomers appear as chains and rings. In rings, each VO_4 tetrahedron is formed by one V=O vanadyl bond, two V-O-V bonds to oxygen atoms shared with neighboring vanadium atoms ('bridging' V-O bonds), and one bond to a surface oxygen atom ('anchoring' V-O bonds). This

also applies to vanadium atoms in chain structures except for the two terminal vanadium atoms, which have one V-O-V bond less. One of these V atoms establishes a V-O-Ce bond by using an O atom stemming from the adsorbed cluster, while the other V atom binds to an additional surface oxygen atom to adopt 4-fold coordination. The corresponding surface oxygen atom is usually significantly displaced from its position in pristine CeO_2(111). This structural feature was described as a so-called "pseudo-oxygen-vacancy" in a previous study.[30] Similar to an actual oxygen vacancy,[60] it serves as a very favorable binding site for methanol and, consequently, enhances the activity of the catalyst.[33] Rings matching the hexagonal surface structure of CeO_2(111), i.e. containing three or six VO_2 units, are very stable and abundant structural motifs (in the GA populations).

Table 1. Mean V-O bond distances[a] (pm) of V_nO_{2n} clusters as well as VO_2 and V_2O_5 MLs on CeO_2(111) using dispersion-corrected PBE+U.

	vanadyl (V=O)	bridging (V-O-V)	anchoring (V-O-Ce)	interphase[b]
VO_2/CeO_2(111)	163	-	181	174
V_2O_4/CeO_2(111)	162	182	180	173
V_3O_6/CeO_2(111)	161	182	174	-
V_4O_8/CeO_2(111)	161	182 (178 – 185)	178 (176 – 180)	173
V_5O_{10}/CeO_2(111)	162 (161-165)	182 (177 – 189)	178 (174 – 180)	172
V_6O_{12}/CeO_2(111)	161	181	175	-
V_7O_{14}/CeO_2(111)	162 (161-165)	181 (178 – 185)	175 (173 – 176)	-
V_8O_{16}/CeO_2(111)	161	184 (165 – 224)	176 (173 – 184)	-
VO_2-ML-a/CeO_2(111)	160	183 (170 – 196)	177 (175 – 179)	-
VO_2-ML-c/CeO_2(111)	160	199 (194 – 201)	176	-
V_2O_5-ML-a/CeO_2(111)	160	189 (170 – 224)	211 (176 – 228)	-

[a] If the smallest and largest distances differ by more than 2 pm, the range is given in parentheses.
[b] V-O-Ce bonds at the end of a chain with a 2-fold coordinated oxygen, commonly involved in formation of a pseudovacancy.

Figure 1 shows only the most stable structure of a given composition which are labeled V_nO_{2n}-a in section 1 of the Supporting Information. The latter provides a more complete account of low energy structures of surface V_nO_{2n} clusters with n = 4 – 8.

The abundance of ring structures for larger oligomers and the associated lack of a pseudovacancy might explain the experimentally observed lower activity for catalysts formed at high vanadia coverage, which feature bigger clusters. In addition, only one pseudovacancy is formed per cluster. Therefore, larger oligomers are probably less active than the monomer, since (i) the pseudovacancy might be harder to access due to steric effects, and (ii) the degree of reduction is higher for larger VO_2 oligomers, rendering further surface reduction during methanol oxidation energetically less favorable.

3.2. Comparison with gas-phase clusters and different supports. Neutral and anionic gas-phase V_nO_m clusters with more than three vanadium atoms prefer to form cage-like structures,[61-63] while the supported VO_2 clusters described above form two-dimensional structures to maximize contact with the surface. Nevertheless, adsorbed clusters and gas-phase clusters have several points in common. In both cases, the predominant coordination number of vanadium atoms is four, and six-membered rings are common structural motifs. Gas-phase clusters often involve eight-membered rings, which were also found on the CeO_2(111) surface. However, they are energetically less favorable than six-membered rings since they do not match the hexagonal lattice of the surface. Regarding the electron distribution, mixed cerium – vanadium oxide clusters in the gas phase show the same preference for the Ce^{3+}/V^{5+} oxidation states as found for the supported clusters.[64]

For a recent review of experimental and theoretical studies on vanadia model catalysts on different supports we refer to ref. 3. On ultrathin Al_2O_3 films grown on a NiAl substrate, cage type, two-layer V_4O_{10} and V_6O_{15} clusters which contain 4-fold coordinated V atoms show up in the stability diagram,[40] in contrast to the flat VO_2 oligomers studied in this work. This is in

agreement with the observed tendency of vanadia on Al_2O_3/NiAl films of forming taller aggregates rather than wetting the surface.[40,65]

Vanadia clusters with V_2O_5 composition on (101) and (001) surfaces of tetragonal ZrO_2 are discussed in ref. 66. V-O bond distances of monomers (vanadyl: 161 *vs.* 163 pm; anchoring: 179 *vs.* 181 pm) and dimers (vanadyl: 161 *vs.* 162 pm; bridging: 185 *vs.* 182 pm; anchoring: 177 *vs.* 180 pm) are similar to those of ceria-supported clusters, and the clusters also contain 4-fold coordinated vanadium. The monomers have been obtained by dissociating V_2O_5 to VO_3^- and VO_2^+. In all these species, vanadium is in the +5 oxidation state.

Although TiO_2 is considered a reducible oxide, it does not stabilize the +5 oxidation state of vanadium to the same extent as ceria does, i.e. $(VO_2)_n$ clusters on titania surfaces mostly contain reduced vanadium cations. Henkelman and coworkers studied monomers, dimers and tetramers on rutile and anatase surfaces.[67] Coordination numbers of V range from three to six.

3.3. VO_2 monolayers. The most stable VO_2 ML structure (VO_2-ML-a, see Figure 2, top) is formed by chains built from a mixture of V_{4c} and V_{5c} atoms. Each V_{4c} (V_{5c}) atom is connected to three V_{5c} (V_{4c}) atoms via bridging O atoms. Two of these connections are in chain direction and the third one is perpendicular to the chain direction. This results in eight-membered $(V\text{-}O\text{-})_4$ rings with C_2 symmetry as structural motifs. In terms of coordination polyhedra, VO_5 trigonal-bipyramids are linked to two tetrahedra by using the pyramid tops and to another tetrahedron by using a vertex of the triangular base, which is perpendicular to the surface. Only the V_{5c} atoms feature vanadyl groups, which are tilted towards the surface (43° with respect to the surface normal). V_{5c} atoms are elevated by 23 pm compared to V_{4c} atoms. The formation of anchoring V-O bonds strongly affects the support structure. Surface oxygen atoms bonded to V_{5c} (V_{4c}) atoms are lifted by 69 pm (43 pm) compared to their position in pristine CeO_2(111). Due to additional lateral displacements of the surface oxygen atoms, the change in O-Ce bond

distances is asymmetric, i.e. instead of three bonds with the same distance (237 pm), the bond distances range from 247 pm to 268 pm.

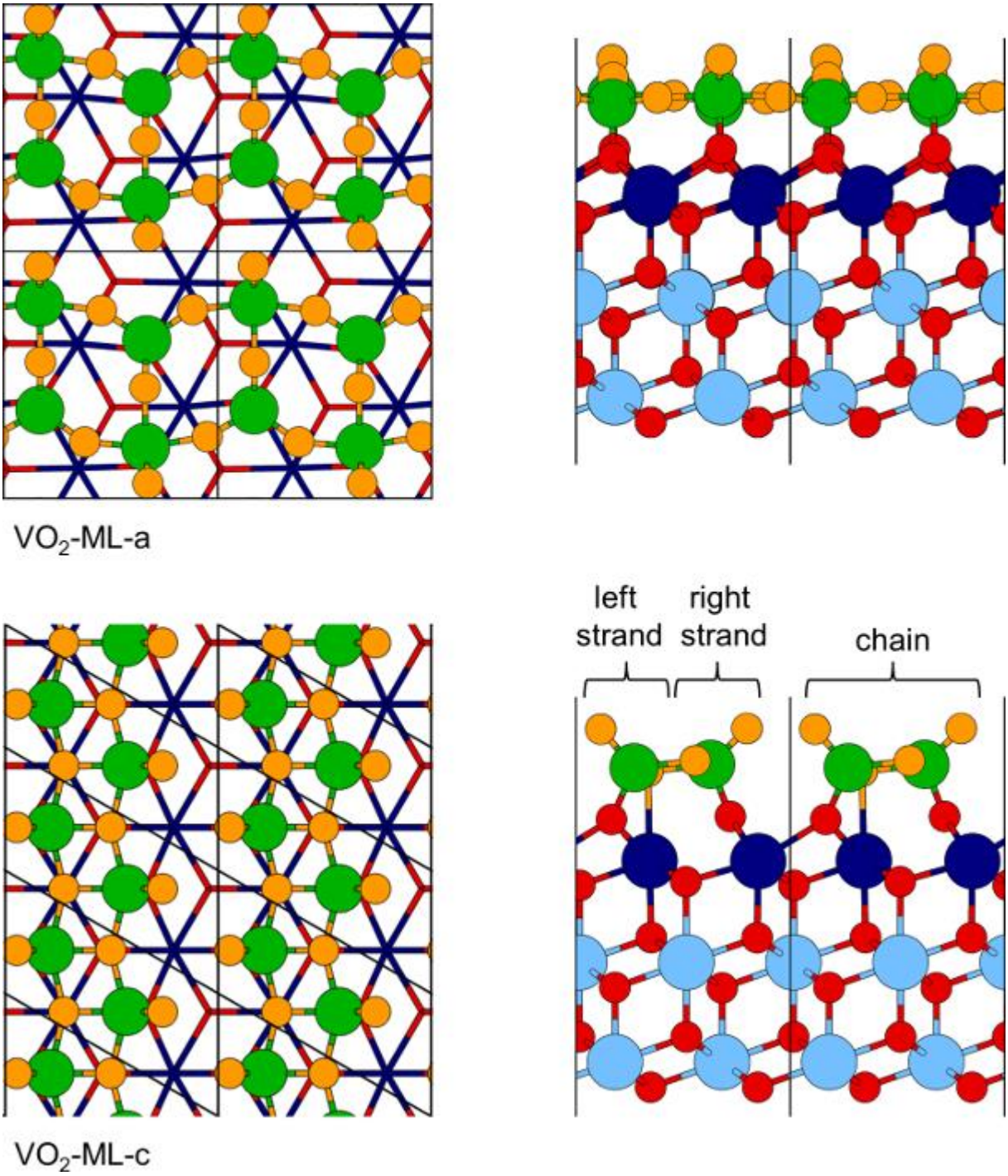

Figure 2. Stable (VO_2-ML-a, top) and a meta-stable structure (VO_2-ML-c, bottom) of the VO_2 ML on CeO_2(111) in top view (left) and side view (right). For details and color code, see Figure 1. Black lines indicate primitive unit cells.

As shown in Figure 2 (top), the primitive unit cell is rectangular and contains four VO_2 units. Placing the same V_4O_8 repeat unit in a rhombic *p*(2x2) CeO_2(111) unit cell results in a different

pattern regarding the connection of the repeat units. In this structure (VO_2-ML-b, see Figure S2), V atoms of one ring are linked to V atoms of different neighboring rings (creating a two-dimensional network of rings), instead of being linked to V atoms of the same neighboring ring (creating chains of fused rings). This structure is 0.05 eV/V atom higher in energy compared to the one shown in Figure 2 (top).

Similar to VO_2 oligomers, the V 3d electron of each VO_2 unit of the adlayer is transferred to Ce^{4+} surface ions. This leads to a reduction of each Ce^{4+} ion in the topmost trilayer to Ce^{3+} while vanadium adopts the oxidation state +5. The structure may therefore be described as a ML of V_2O_5 on a Ce_2O_3 surface layer on CeO_2. The (111) surface of the cubic bulk phase of Ce_2O_3 (c-Ce_2O_3, bixbyite) and the (0001) surface of Ce_2O_3 have a hexagonal surface structure closely resembling that of CeO_2(111). Experimental results show that reducing CeO_2(111) films creates ordered surface layers of Ce_2O_3.[68-70] The transformation of CeO_2(111) to Ce_2O_3(0001) has been discussed in ref. 71.

A different VO_2 ML structure (VO_2-ML-c, see Figure 2, bottom) was also considered due to its similarities with the chains formed by VO_3^- in hydrated metavanadates, e.g. $KVO_3 \cdot H_2O$, and the (001) surface structure of V_2O_5. This structure has a similar V_2O_5-type motif as the monolayer structure reported for VO_2 on ZrO_2(101).[66]

Figure 3 provides a more detailed comparison. Compared to VO_2-ML-a, it is 0.20 eV/V atom higher in energy. The constituent VO_2 units are placed with their V-O bond parallel to the surface and the vanadyl bond adopts a tilt angle of 41° to 45° with respect to the surface normal. Along the direction of one surface cell vector, the VO_2 units are stacked in an alternating pattern, which results in the formation of parallel infinite chains. The orientation of these chains with respect to the support is perpendicular to the chain direction in the most stable VO_2 ML structure. Vanadium is 5-fold coordinated, and the distorted VO_5 trigonal-bipyramids share two edges with neighboring units. The repeat unit contains four-membered $(V\text{-}O\text{-})_2$ rings as a structural motif, in contrast to the $(V\text{-}O\text{-})_4$ rings in the most stable structure. Oxygen atoms of

the VO_2 layer are either connected to a single vanadium atom via a vanadyl bond or to three V atoms as part of the chains. Each chain can be divided into two strands, which will be labeled 'left' and 'right' according to Figure 2 (bottom). The O atoms in the left strand are in atop position of a surface Ce atom, with an average O-Ce distance of 281 pm. In contrast, the O atoms of the right strand are located above a subsurface O atom. V atoms are bonded to two O atoms of their strand and one O atom from the other strand. Surface oxygen atoms connected to the left (right) strand of the VO_2 ML are lifted by 54 pm (63 pm) compared to their position in pristine CeO_2(111). Furthermore, they are displaced laterally, breaking the symmetric coordination in pristine CeO_2 with three O-Ce distances of 237 pm. Surface oxygen atoms connected to the left strand of the VO_2 ML feature one short (249 pm) and two long (261 pm) O-Ce distances, while surface oxygen atoms connected to the right strand feature one large (288 pm) and two small (254 pm) O-Ce distances.

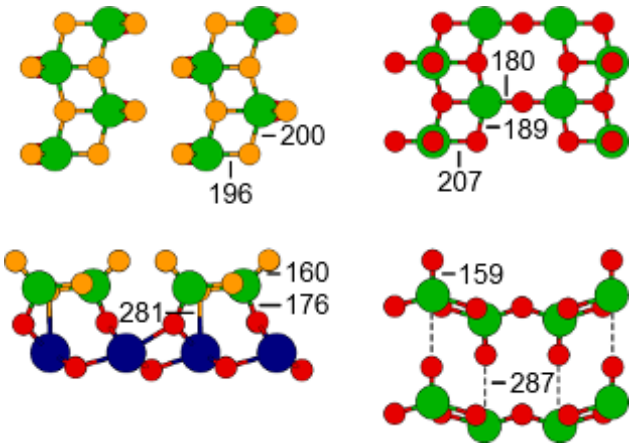

Figure 3. Comparison of the VO_2-ML-c (left) to V_2O_5(001) (right) in top view (top) and side view (bottom). Bond distances are given in pm. For details and color code, see Figure 1.

3.4. V_2O_5 monolayer. The most stable structure found for the fully oxidized V_2O_5 ML is shown in Figure 4. It was obtained by adding oxygen atoms between the chains of VO_2-ML-c, followed by simulated annealing. The same structure was also obtained by addition of oxygen atoms between the chains of VO_2-ML-a and local optimization. It contains equal numbers of 6-fold

and 4-fold coordinated vanadium atoms. V_{6c} atoms form chains of distorted corner-sharing VO_6 octahedra. Between these rows of octahedra, pairs of corner-sharing VO_4 tetrahedra are placed. Only one vanadium atom of the pair features a vanadyl bond. This vanadium atom is not bound to a surface oxygen atom and is vertically lifted by 66 pm compared to V_{6c} atoms. It will be referred to as V^{u}_{4c} (u for 'upper atom'). The other vanadium atom of the pair is bound to a surface oxygen atom instead, i.e. it does not have a vanadyl bond. These V_{4c} atoms without a vanadyl bond will be referred to as V^{l}_{4c} (l for 'lower atom'). They are located 12 pm closer to the surface than V_{6c} atoms. To summarize, parallel chains of corner-sharing VO_6 octahedra are connected by sharing vertices with pairs of corner-sharing tetrahedra. Vanadium oxide frameworks built from a mixture of octahedra and tetrahedra are known to exist,[72] but this specific arrangement has to the best of our knowledge not been described in the literature so far.

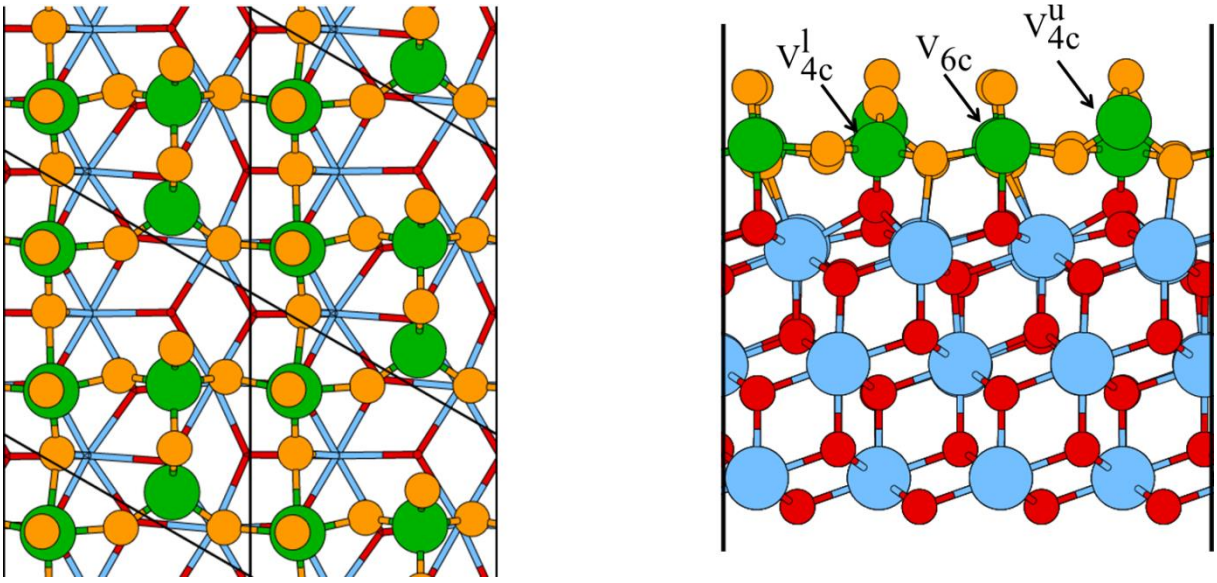

Figure 4. V_2O_5 ML on $CeO_2(111)$ in top view (left) and side view (right). The side view indicates the three different types of V^{5+} cations, with the subscript denoting the coordination number and the superscript referring to lower ('l') and upper ('u'). For details and color code, see Figure 1.

The coordination polyhedra are rather distorted and feature multiple V-O bond distances (see Figure 5). In contrast to the VO_2 ML, which involves large displacements of surface oxygen atoms, the support structure is mostly unaffected by deposition of the V_2O_5 ML. Only surface O atoms bonded to V^{l}_{4c} atoms are significantly displaced from their position in pristine CeO_2(111), while $^1/_4$ of the surface oxygen atoms are not connected to the vanadium oxide adlayer.

The tetrahedra pairs can be arranged in two patterns. In the first one, which is shown in Figure 4, V_{4c} atoms are out of registry, i.e. V^{u}_{4c} and V^{l}_{4c} atoms alternate perpendicular to the octahedra chains, so that each V_{6c} atom is bonded to one V^{u}_{4c} and one V^{l}_{4c}. The other pattern (see Figure S3) has V_{4c} atoms that are in registry, so that each V_{6c} atom is bonded to either two V^{u}_{4c} or two V^{l}_{4c}. The energy difference between these two structures is negligibly small (2 meV/V atom). The patterns correspond to the two different VO_2 ML arrangements (VO_2-ML-a and VO_2-ML-b) described above. Adding one bridging O atom between certain V_{4c} and V_{5c} atoms as well as a vanadyl O atom to the corresponding V_{4c} atom transforms the VO_2 ML to the V_2O_5 ML.

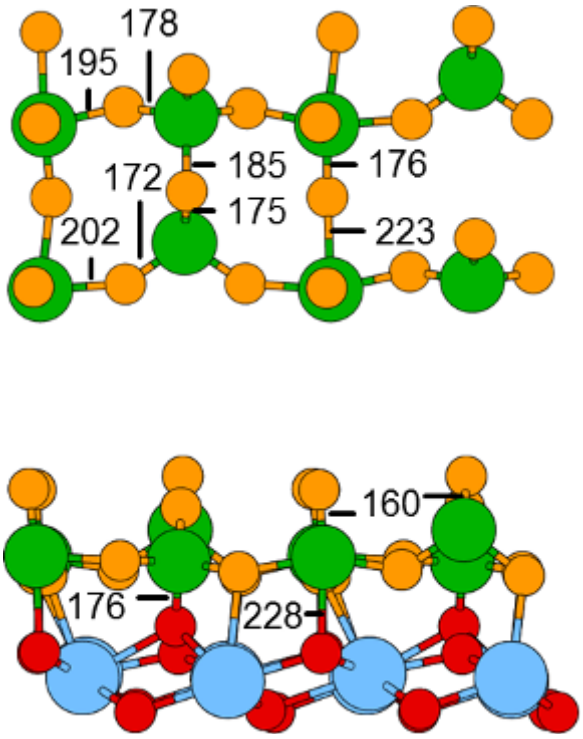

Figure 5. Bond distances (pm) in the V_2O_5 ML on $CeO_2(111)$ in top view (top) and side view (bottom). For details and color code, see Figure 1.

3.5. Relative stabilities of oligomers and monolayers.

Table 2 shows relative stabilities of the VO_2 surface aggregates compared to bulk VO_2 and V_2O_5 per VO_2 unit.

$$\{VO_2\}_{bulk} + \frac{1}{n}\{(CeO_2)_{48}\} \rightarrow \frac{1}{n}\{V_nO_{2n}\cdot(CeO_2)_{48}\} \quad (1a)$$

$$\frac{1}{2}\{V_2O_5\}_{bulk} + \frac{1}{n}\{(CeO_2)_{48}\} \rightarrow \frac{1}{n}\{V_nO_{2n}\cdot(CeO_2)_{48}\} + \frac{1}{4}O_2 \quad (1b)$$

The energies according to eq. (1b) differ from (1a) by the bulk reduction energy, i.e. the energy required to form VO_2 and O_2 from V_2O_5. Using our calculated values (per V atom), this amounts to adding 0.75 eV to the relative stabilities according to eq. (1a) in Table 2. For example, in the

case of the VO_2 monolayer, the resulting reaction energy is +0.07 eV, implying a slight thermodynamic preference of bulk V_2O_5 compared to surface VO_2 species.

Agglomeration energies,

$$\{VO_2 \cdot (CeO_2)_{48}\} \rightarrow \frac{1}{n}\{V_nO_{2n} \cdot (CeO_2)_{48}\} + \frac{n-1}{n}\{(CeO_2)_{48}\} \quad (2)$$

relate the stability of an aggregate to the smallest building block. They are obtained from the relative stabilities, eq. 1a, by just subtracting the relative stability of the VO_2 monomers which are able to diffuse and agglomerate. For example, the agglomeration energy (Table 2) for the trimer is -0.74 – (-0.08) = -0.66 eV.

Growth energies,

$$\{VO_2 \cdot (CeO_2)_{48}\} + \{V_{n-1}O_{2n-2} \cdot (CeO_2)_{48}\} \rightarrow \{V_nO_{2n} \cdot (CeO_2)_{48}\} + \{(CeO_2)_{48}\} \quad (3)$$

describe the energy gain when adding a monomer to an existing oligomer.

Table 2. Relative stabilities and growth energies (eq. 3) in eV for V_nO_{2n} aggregates on CeO_2(111).

n	Relative stability		Growth energy
	(eq. 1a)	(eq. 1b)	(eq. 3)
1	-0.08	+0.67	0
2	-0.58	+0.17	-0.99
3	-0.74	±0.00	-1.00
4	-0.73	+0.02	-0.62
5	-0.64	+0.11	-0.18
6	-0.73	+0.02	-1.13
7	-0.68	+0.07	-0.30
8	-0.63	+0.11	-0.20
16 (ML)	-0.68	+0.07	-

Table 2 shows that combining monomers to form any of the higher oligomers and, ultimately, a ML, is an exothermic process. However, there are three systems with particularly high agglomeration energies: the trimer, the tetramer, and the hexamer.

In addition to the agglomeration energies presented in Table 2, relative stabilities of the different supported vanadia species have also been analyzed using free energies calculated from DFT energies and molecular statistics. Examples of applying these approaches to solid-state systems can be found in refs. 44,66,73. Details concerning our specific set of equations and approximations are described in ref. 29. Zero-point vibrational contributions and thermal vibrational contributions were neglected. For a comprehensive picture, adsorbed VO species as well as oxygen-defective VO and VO_2 oligomers studied in ref. 29 have also been included. In addition, oxygen-defective ML structures have been generated and incorporated as well. The resulting stability diagram (phase diagram) is shown in Figure 6. It is dominated by ML structures, especially the VO_2 ML. This confirms the previously reported thermodynamic preference of VO_2 units to aggregate and indicates that vanadia wets the ceria surface completely. Relative stabilities of the different ML structures suggest that the VO_2 ML is more relevant than the V_2O_5 ML under UHV conditions. This is in agreement with observation detecting an increasing number of Ce^{3+} ions with increasing vanadium coverage. Compared with the corresponding bulk phases, a much larger oxygen partial pressure is required to oxidize VO_2 to V_2O_5 supported on CeO_2(111), which illustrates the stabilizing effect of the support.

The trimer and hexamer rings presented in Figure 1 also show up in the phase diagram which is compatible with the observed STM images which, at higher vanadium coverage, show two predominant species consisting of rings formed by three and six protrusions, respectively.[21]

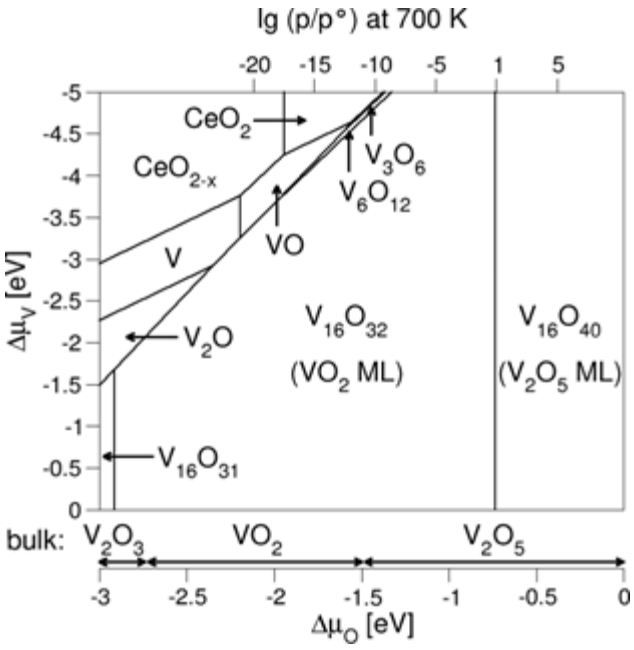

Figure 6. Phase diagram of various adsorbed vanadia clusters. The Figure shows the most stable species as a function of $\Delta\mu_V$ and $\Delta\mu_O$. The latter has been translated into an oxygen pressure scale at 700 K. For comparison, the most stable bulk phase as a function of $\Delta\mu_O$ is shown at the bottom (calculated values).

Under catalytic reaction conditions, vanadia supported on ceria may convert into the stable cerium vanadate phase, $CeVO_4$, see, e.g. ref. 74, for which a $Ce(f^1)^{III+}/V(d^0)^{V+}$ electronic structure has been predicted using PBE+U[75] in agreement with the earlier interpretation of XANES spectra.[76] Therefore, we look at the relative stability of our most stable monolayer phase, VO_2-ML-a, with respect to bulk $CeVO_4$ which, taking into account the composition of our slab models, is expressed by the reaction

$$\frac{1}{16}\{(VO_2)_{16}\cdot(CeO_2)_{48}\} \rightarrow \{CeVO_4\}_{bulk} + \frac{1}{24}\{(CeO_2)_{48}\} \qquad (4)$$

Within our assumptions (no vibrational contributions to chemical potential differences) the free energy differences are identical with the energy differences at 0K. The reaction energy, -1.09 eV, indicates a thermodynamically very favorable formation of cerium vanadate, which is in qualitative agreement with experiment.[74]

3.6. Infrared spectra

Infrared reflection absorption spectroscopy (IRAS) experiments indicate the presence of terminal vanadyl (V=O) bonds.[21] Upon increasing vanadia coverage,, the wavenumber of the V=O stretching mode is shifted from 1006 cm^{-1} (predominantly monomers) to 1033 cm^{-1} (trimers) to 1040 cm^{-1} for larger aggregates.[65] This shift is attributed to a coupling of the V=O dipole moments. As already reported in earlier work,[29] the blue-shift from monomeric to trimeric species is reproduced by the calculated harmonic vibrational wavenumbers (Table 3) which are systematically to high – a known phenomenon for the type of functional used. However, Table 3 shows that an increase in cluster size is not always connected with a blue-shift of the V=O stretching mode. Test calculations indicate that not only vanadium atoms within an adsorbed cluster may influence the vibrational frequencies, but also nearby clusters. In particular, the most intense V=O stretching mode of V_3O_6 clusters is blue-shifted by 12 cm^{-1} upon doubling the V coverage, i.e. depositing two clusters per $p(4 \times 4)$ unit cell.

The wavenumbers calculated for the V=O stretching modes of the most stable VO_2 monolayer (VO_2-ML-a) are very close to the ones of the largest, V_8O_{16} cluster. Both the calculated (1072 cm^{-1}) and observed (1040 cm^{-1}) wavenumbers of the V=O vibrations of vanadyl-terminated V_2O_3(0001) surface[77] are very close to the respective values for the large VO_2 aggregates (calc. 1069, obsd. 1040 cm^{-1}). The calculated V=O stretching wavenumbers fall also in the range of values calculated for the most stable V_2O_5 layer on an ultrathin $Al_2O_{2.6}$ film grown on a NiAl substrate,[40] and for the V_2O_5 (001) surface.

Table 3. Harmonic wavenumbers (cm^{-1}) of V=O stretch vibrations of V_nO_{2n} clusters and monolayers on $CeO_2(111)$ using dispersion-corrected PBE+U compared to other systems and experiment.

	range	most intense
$VO_2/CeO_2(111)$	1024	1024
$V_2O_4/CeO_2(111)$	1025-1035	1025
$V_3O_6/CeO_2(111)$	1049-1063	1049[a]
$V_4O_8/CeO_2(111)$	1036-1058	1045;1058
$V_5O_{10}/CeO_2(111)$	1025-1035	1027
$V_6O_{12}/CeO_2(111)$	1045-1067	1048
$V_7O_{14}/CeO_2(111)$	957-1065	1054
$V_8O_{16}/CeO_2(111)$	1039-1069	1069
VO_2-ML-a/$CeO_2(111)$	1060-1069	1060;1069
VO_2-ML-c/$CeO_2(111)$	1054-1092	1054;1058
V_2O_5-ML-a/$CeO_2(111)$	1047-1082	1047
O-$V_2O_3(0001)$		1072[b]
$V_2O_5/Al_2O_{2.6}$	1033-1088[c]	
$V_2O_5(001)$	1066-1102[d]	1102

[a] Shifted to 1061 cm^{-1} upon placing a second V_3O_6 cluster in the $p(4 \times 4)$ unit cell.
[b] Vanadyl-covered $V_2O_3(0001)$ surface, unscaled value from ref. 77.
[c] Ref. 40.
[d] Ref. 38: 1042-1095 cm^{-1}.

4. Conclusions

Vanadia oligomers, $(VO_2)_n$, deposited on $CeO_2(111)$ mainly contain tetrahedrally coordinated V^{5+} ions as principal building blocks. One electron per VO_2 unit is transferred to the support creating n Ce^{3+} ions, leading to a $(VO_2^+)_n/CeO_2(111)^{n-}$ system. With increasing coverage, especially with respect to monolayer formation, V atoms with larger coordination numbers (five or six) become more abundant. Likewise, monolayer structures feature more bridging V-O-V bonds. Furthermore, V atoms in small oligomers are preferentially vanadyl-terminated, while some V atoms in large oligomers and the monolayer structures lack V=O groups. The preference for monolayer aggregates from small clusters to full surface coverage together with the fact that flat "monolayer" clusters are preferred to taller "bilayer" clusters, i.e. for wetting the ceria surface, is in contrast to what has been found for non-reducible oxides such as alumina.

Pseudo-oxygen vacancies, i.e. oxygen ions lifted out of the surface to anchor the vanadia cluster, are present in most of the chain-type oligomers, but are absent in ring structures and the monolayer structures. Upon increasing cluster size, these pseudovacancies become less abundant, in agreement with the experimentally observed lower activity at higher V loading of the CeO_2(111) support.

Agglomeration of adsorbed VO_2 units is strongly exothermic, and VO_2 monolayer structures are predicted to be thermodynamically favorable under a wide range of experimentally relevant conditions (vanadium oxide loading and oxygen partial pressure).

ASSOCIATED CONTENT

Supporting Information

The Supporting Information is available free of charge on the ACS Publication website at DOI: xxx.xxx

Additional VO_2 and V_2O_5 monolayer structures; total energies of all optimized structures; x,y,z coordinates of optimized structures.

AUTHOR INFORMATION

Corresponding Author

*E-mail: js@chemie.hu-berlin.de.

ORCID

Christopher Penschke 0000-0002-0117-7479

Joachim Paier 0000-0001-6085-2211

Joachim Sauer 0000-0001-6798-6212

Present Address

† C.P.: Department of Physics and Astronomy, University College London, Gower Street, London WC1E 6BT, United Kingdom.

Notes

The authors declare no competing financial interest.

ACKNOWLEDGEMENTS

The authors are grateful for computing time at the high-performance computer centers HLRN (North-German Super-computing Alliance in Berlin and Hannover). We acknowledge support from the German Research Foundation within the Cluster of Excellence "Unifying Concepts in Catalysis" (EXC314), COST action CM1104, and the "Fonds der Chemischen Industrie".

REFERENCES

1. Weckhuysen, B. M.; Keller, D. E. Chemistry, Spectroscopy and the Role of Supported Vanadium Oxides in Heterogeneous Catalysis. *Catal. Today* **2003,** *78*, 25-46.
2. Wachs, I. E. Recent Conceptual Advances in the Catalysis Science of Mixed Metal Oxide Catalytic Materials. *Catal. Today* **2005,** *100*, 79-94.
3. Artiglia, L.; Agnoli, S.; Granozzi, G. Vanadium Oxide Nanostructures on Another Oxide: The Viewpoint from Model Catalysts Studies. *Coord. Chem. Rev.* **2015,** *301*, 106-122.
4. Deo, G.; Wachs, I. E. Reactivity Of Supported Vanadium-Oxide Catalysts - The Partial Oxidation Of Methanol. *J. Catal.* **1994,** *146*, 323-334.
5. Wachs, I. E.; Deo, G.; Juskelis, M. V.; Weckhuysen, B. M., Methanol Oxidation. In *Dynamics of Surfaces and Reaction Kinetics in Heterogeneous Catalysis*, Froment, G. F.; Waugh, K. C., Eds. Elsevier: Amsterdam, **1997**; pp 305-314.
6. Wachs, I. E.; Chen, Y.; Jehng, J.-M.; Briand, L. E.; Tanaka, T. Molecular Structure and Reactivity of the Group V Metal Oxides. *Catal. Today* **2003,** *78*, 13-24.
7. Wachs, I. E. In *Catalysis*, Spivey, J. J., Ed. The Royal Society of Chemistry: 1997; p 37.
8. Wong, G. S.; Concepcion, M. R.; Vohs, J. M. Oxidation of Methanol to Formaldehyde on Vanadia Films Supported on CeO_2(111). *J. Phys. Chem. B* **2002,** *106*, 6451-6455.
9. Feng, T.; Vohs, J. M. A TPD Study of the Partial Oxidation of Methanol to Formaldehyde on CeO2-Supported Vanadium Oxide. *J. Catal.* **2004,** *221*, 619-629.
10. Artiglia, L.; Agnoli, S.; Vittadini, A.; Verdini, A.; Cossaro, A.; Floreano, L.; Granozzi, G. Atomic Structure and Special Reactivity Toward Methanol Oxidation of Vanadia Nanoclusters on TiO_2(110). *J. Am. Chem. Soc.* **2013,** *135*, 17331-17338.
11. Beck, B.; Harth, M.; Hamilton, N. G.; Carrero, C.; Uhlrich, J. J.; Trunschke, A.; Shaikhutdinov, S.; Schubert, H.; Freund, H.-J.; Schlögl, R., et al. Partial Oxidation of Ethanol on Vanadia Catalysts on Supporting Oxides with Different Redox Properties Compared to Propane. *J. Catal.* **2012,** *296*, 120-131.
12. Artiglia, L.; Agnoli, S.; Savio, L.; Pal, J.; Celasco, E.; Rocca, M.; Bondino, F.; Magnano, E.; Castellarin-Cudia, C.; Netzer, F. P., et al. From Vanadia Nanoclusters to Ultrathin Films on TiO_2(110): Evolution of the Yield and Selectivity in the Ethanol Oxidation Reaction. *ACS Catal.* **2014,** *4*, 3715-3723.
13. Andrushkevich, T. V.; Kaichev, V. V.; Chesalov, Y. A.; Saraev, A. A.; Buktiyarov, V. I. Selective Oxidation of Ethanol over Vanadia-Based Catalysts: The Influence of Support Material and Reaction Mechanism. *Catal. Today* **2017,** *279*, 95-106.
14. Carrero, C. A.; Schlögl, R.; Wachs, I. E.; Schomäcker, R. Critical Literature Review of the Kinetics for the Oxidative Dehydrogenation of Propane over Well-Defined Supported Vanadium Oxide Catalysts. *ACS Catal.* **2014,** *4*, 3357-3380.
15. Khodakov, A.; Olthof, B.; Bell, A. T.; Iglesia, E. Structure and Catalytic Properties of Supported Vanadium Oxides: Support Effects on Oxidative Dehydrogenation Reactions. *J. Catal.* **1999,** *181*, 205-216.

16. Olthof, B.; Khodakov, A.; Bell, A. T.; Iglesia, E. Effects of Support Composition and Pretreatment Conditions on the Structure of Vanadia Dispersed on SiO_2, Al_2O_3, TiO_2, ZrO_2, and HfO_2. *J. Phys. Chem. B* **2000,** *104*, 1516-1528.
17. Iglesias-Juez, A.; Martínez-Huerta, M. V.; Rojas-García, E.; Jehng, J. M.; Bañares, M. A. On the Nature of the Unusual Redox Cycle at the Vanadia Ceria Interface. *J. Phys. Chem. C* **2018,** *122*, 1197-1205.
18. Vohs, J. M.; Feng, T.; Wong, G. S. Comparison of the Reactivity of High-Surface Area, Monolayer Vanadia/Ceria Catalysts with Vanadia/CeO_2(111) Model Systems. *Catal. Today* **2003,** *85*, 303-309.
19. Ganduglia-Pirovano, M. V.; Popa, C.; Sauer, J.; Abbott, H. L.; Uhl, A.; Baron, M.; Stacchiola, D.; Bondarchuk, O.; Shaikhutdinov, S.; Freund, H.-J. Role of Ceria in Oxidative Dehydrogenation on Supported Vanadia Catalysts. *J. Am. Chem. Soc.* **2010,** *132*, 2345-2349.
20. Sauer, J.; Freund, H. J. Models in Catalysis. *Catal. Lett.* **2015,** *145*, 109-125.
21. Baron, M.; Abbott, H.; Bondarchuk, O.; Stacchiola, D.; Uhl, A.; Shaikhutdinov, S.; Freund, H.-J.; Popa, C.; Ganduglia-Pirovano, M. V.; Sauer, J. Resolving the Atomic Structure of Vanadia Monolayer Catalysts: Monomers, Trimers, and Oligomers on Ceria. *Angew. Chem.-Int. Edit.* **2009,** *48*, 8006-8009.
22. Burcham, L.; Deo, G.; Gao, X.; Wachs, I. In Situ IR, Raman, and UV-Vis DRS Spectroscopy of Supported Vanadium Oxide Catalysts During Methanol Oxidation. *Top. Catal.* **2000,** *11-12*, 85-100.
23. Burcham, L. J.; Wachs, I. E. The Origin of the Support Effect in Supported Metal Oxide Catalysts: In Situ Infrared and Kinetic Studies During Methanol Oxidation. *Catal. Today* **1999,** *49*, 467-484.
24. Abbott, H. L.; Uhl, A.; Baron, M.; Lei, Y.; Meyer, R. J.; Stacchiola, D. J.; Bondarchuk, O.; Shaikhutdinov, S.; Freund, H. J. Relating Methanol Oxidation to the Structure of Ceria-Supported Vanadia Monolayer Catalysts. *J. Catal.* **2010,** *272*, 82-91.
25. Sturm, J. M.; Göbke, D.; Kuhlenbeck, H.; Döbler, J.; Reinhardt, U.; Ganduglia-Pirovano, M. V.; Sauer, J.; Freund, H. J. Partial Oxidation of Methanol on Well-Ordered V_2O_5(001)/Au(111) Thin Films. *Phys. Chem. Chem. Phys.* **2009,** *11*, 3290-3299.
26. Wachs, I. E. Catalysis Science of Supported Vanadium Oxide Catalysts. *Dalton Trans.* **2013,** *42*, 11762-11769.
27. Wong, G. S.; Vohs, J. M. An XPS Study of the Growth and Electronic Structure of Vanadia Films Supported on CeO_2(111). *Surf. Sci.* **2002,** *498*, 266-274.
28. Popa, C.; Ganduglia-Pirovano, M. V.; Sauer, J. Periodic Density Functional Theory Study of VO_n Species Supported on the CeO_2(111) Surface. *J. Phys. Chem. C* **2011,** *115*, 7399-7410.
29. Penschke, C.; Paier, J.; Sauer, J. Oligomeric Vanadium Oxide Species Supported on the CeO_2(111) Surface: Structure and Reactivity Studied by Density Functional Theory. *J. Phys. Chem. C* **2013,** *117*, 5274-5285.
30. Paier, J.; Kropp, T.; Penschke, C.; Sauer, J. Stability and Migration Barriers of Small Vanadium Oxide Clusters on the CeO_2(111) Surface Studied by Density Functional Theory. *Faraday Discuss.* **2013,** *162*, 233-245.
31. Döbler, J.; Pritzsche, M.; Sauer, J. Oxidation of Methanol to Formaldehyde on Supported Vanadium Oxide Catalysts Compared to Gas Phase Molecules. *J. Am. Chem. Soc.* **2005,** *127*, 10861-10868.
32. Rozanska, X.; Fortrie, R.; Sauer, J. Oxidative Dehydrogenation of Propane by Monomeric Vanadium Oxide Sites on Silica Support. *J. Phys. Chem. C* **2007,** *111*, 6041-6050.
33. Kropp, T.; Paier, J.; Sauer, J. Support Effect in Oxide Catalysis: Methanol Oxidation on Vanadia/Ceria. *J. Am. Chem. Soc.* **2014,** *136*, 14616-14625.
34. T. Kropp; J. Paier; Sauer, J. Oxidative Dehydrogentation of Methanol at Ceria-supported Vanadia Oligomers. *J. Catal.* **2017,** *352*, 382-387.
35. Wu, X. P.; Gong, X. Q. Unique Electronic and Structural Effects in Vanadia/Ceria-Catalyzed Reactions. *J. Am. Chem. Soc.* **2015,** *137*, 13228-13231.
36. Wu, X. P.; Liu, J. J.; Fan, J.; Gong, X. Q. Theoretical Studies on the Monomeric Vanadium Oxides Supported by Ceria: The Atomic Structures and Oxidative Dehydrogenation Activities. *RSC Adv.* **2015,** *5*, 52259-52263.

37. Alexopoulos, K.; Hejduk, P.; Witko, M.; Reyniers, M. F.; Marin, G. B. Theoretical Study of the Effect of (001) TiO_2 Anatase Support on V_2O_5. *J. Phys. Chem. C* **2010,** *114*, 3115-3130.
38. Brazdova, V.; Ganduglia-Pirovano, M. V.; Sauer, J. Periodic Density Functional Study on Structural and Vibrational Properties of Vanadium Oxide Aggregates. *Phys. Rev. B* **2004,** *69*, 165420.
39. Todorova, T. K.; Ganduglia-Pirovano, M. V.; Sauer, J. Vanadium Oxides on Aluminum Oxide Supports. 3. Metastable κ-Al_2O_3(001) Compared to α-Al_2O_3(0001). *J. Phys. Chem. C* **2007,** *111*, 5141-5153.
40. Brazdova, V.; Ganduglia-Pirovano, M. V.; Sauer, J. Vanadia Aggregates on an Ultrathin Aluminum Oxide Film on NiAl(110). *J. Phys. Chem. C* **2010,** *114*, 4983-4994.
41. Sayle, D. C.; Catlow, C. R. A.; Perrin, M. A.; Nortier, P. Computer Modeling of the V_2O_5/TiO_2 Interface. *J. Phys. Chem.* **1996,** *100*, 8940-8945.
42. Vittadini, A.; Selloni, A. Periodic Density Functional Theory Studies of Vanadia-Titania Catalysts: Structure and Stability of the Oxidized Monolayer. *J. Phys. Chem. B* **2004,** *108*, 7337-7343.
43. Da Silva, J. L. F.; Ganduglia-Pirovano, M. V.; Sauer, J.; Bayer, V.; Kresse, G. Hybrid Functionals Applied to Rare Earth Oxides: The Example of Ceria. *Phys. Rev. B* **2007,** *75*, 045121.
44. Todorova, T. K.; Ganduglia-Pirovano, M. V.; Sauer, J. Vanadium Oxides on Aluminum Oxide Supports. 1. Surface Termination and Reducibility of Vanadia Films on α-Al_2O_3(0001). *J. Phys. Chem. B* **2005,** *109*, 23523-23531.
45. Włodarczyk, R.; Sierka, M.; Kwapień, K.; Sauer, J.; Carrasco, E.; Aumer, A.; Gomes, J. F.; Sterrer, M.; Freund, H.-J. Structures of the Ordered Water Monolayer on MgO(001). *J. Phys. Chem. C* **2011,** *115*, 6764-6774.
46. Blöchl, P. E. Projector Augmented-Wave Method. *Phys. Rev. B* **1994,** *50*, 17953-17979.
47. Kresse, G.; Joubert, D. From Ultrasoft Pseudopotentials to the Projector Augmented-Wave Method. *Phys. Rev. B* **1999,** *59*, 1758-1775.
48. Kresse, G.; Furthmüller, J. Efficient Iterative Schemes for Ab Initio Total-Energy Calculations Using a Plane-Wave Basis Set. *Phys. Rev. B* **1996,** *54*, 11169-11186.
49. Kresse, G.; Furthmüller, J. Efficiency of Ab-Initio Total Energy Calculations for Metals and Semiconductors Using a Plane-Wave Basis Set. *Comp. Mater. Sci.* **1996,** *6*, 15-50.
50. Liechtenstein, A. I.; Anisimov, V. I.; Zaanen, J. Density-Functional Theory and Strong-Interactions - Orbital Ordering in Mott-Hubbard Insulators. *Phys. Rev. B* **1995,** *52*, R5467-R5470.
51. Anisimov, V. I.; Zaanen, J.; Andersen, O. K. Band Theory and Mott Insulators - Hubbard-U Instead of Stoner-I. *Phys. Rev. B* **1991,** *44*, 943-954.
52. Perdew, J. P.; Ernzerhof, M.; Burke, K. Rationale for Mixing Exact Exchange with Density Functional Approximations. *J. Chem. Phys.* **1996,** *105*, 9982-9985.
53. Dudarev, S. L.; Botton, G. A.; Savrasov, S. Y.; Humphreys, C. J.; Sutton, A. P. Electron-Energy-Loss Spectra and the Structural Stability of Nickel Oxide: An LSDA+U Study. *Phys. Rev. B* **1998,** *57*, 1505-1509.
54. Bengone, O.; Alouani, M.; Blöchl, P.; Hugel, J. Implementation of the Projector Augmented-Wave LDA+U Method: Application to the Electronic Structure of NiO. *Phys. Rev. B* **2000,** *62*, 16392-16401.
55. Grimme, S. Semiempirical GGA-Type Density Functional Constructed with a Long-Range Dispersion Correction. *J. Comput. Chem.* **2006,** *27*, 1787-1799.
56. Bucko, T.; Hafner, J.; Lebegue, S.; Angyan, J. G. Improved Description of the Structure of Molecular and Layered Crystals: Ab Initio DFT Calculations with van der Waals Corrections. *J. Phys. Chem. A* **2010,** *114*, 11814-11824.
57. Kerber, T.; Sierka, M.; Sauer, J. Application of Semiempirical Long-Range Dispersion Corrections to Periodic Systems in Density Functional Theory. *J. Comput. Chem.* **2008,** *29*, 2088-2097.
58. Porezag, D.; Pederson, M. R. Infrared Intensities and Raman-Scattering Activities within Density-Functional Theory. *Phys. Rev. B* **1996,** *54*, 7830-7836.
59. Kokalj, A. Computer Graphics and Graphical User Interfaces as Tools in Simulations of Matter at the Atomic Scale. *Comp. Mater. Sci.* **2003,** *28*, 155-168.

60. Beste, A.; Mullins, D. R.; Overbury, S. H.; Harrison, R. J. Adsorption and Dissociation of Methanol on the Fully Oxidized and Partially Reduced (111) Cerium Oxide Surface: Dependence on the Configuration of the Cerium 4f Electrons. *Surf. Sci.* **2008,** *602*, 162-175.
61. Vyboishchikov, S. F.; Sauer, J. $(V_2O_5)_n$ Gas-Phase Clusters (n=1-12) Compared to V_2O_5 Crystal: DFT Calculations. *J. Phys. Chem. A* **2001,** *105*, 8588-8598.
62. Asmis, K. R.; Santambrogio, G.; Brümmer, M.; Sauer, J. Polyhedral Vanadium Oxide Cages: Infrared Spectra of Cluster Anions and Size-Induced d-Electron Localization. *Angew. Chem.* **2005,** *117*, 3182-3185.
63. Santambrogio, G.; Brummer, M.; Woste, L.; Döbler, J.; Sierka, M.; Sauer, J.; Meijer, G.; Asmis, K. R. Gas Phase Vibrational Spectroscopy of Mass-Selected Vanadium Oxide Anions. *Phys. Chem. Chem. Phys.* **2008,** *10*, 3992-4005.
64. Jiang, L.; Wende, T.; Claes, P.; Bhattacharyya, S.; Sierka, M.; Meijer, G.; Lievens, P.; Sauer, J.; Asmis, K. R. Electron Distribution in Partially Reduced Mixed Metal Oxide Systems: Infrared Spectroscopy of $Ce_mV_nO_o^+$ Gas-Phase Clusters. *J. Phys. Chem. A* **2011,** *115*, 11187-11192.
65. Magg, N.; Immaraporn, B.; Giorgi, J. B.; Schroeder, T.; Bäumer, M.; Döbler, J.; Wu, Z. L.; Kondratenko, E.; Cherian, M.; Baerns, M., et al. Vibrational Spectra of Alumina- and Silica-Supported Vanadia Revisited: An Experimental and Theoretical Model Catalyst Study. *J. Catal.* **2004,** *226*, 88-100.
66. Hofmann, A.; Ganduglia-Pirovano, M. V.; Sauer, J. Vanadia and Water Coadsorption on Tetragonal Zirconia Surfaces. *J. Phys. Chem. C* **2009,** *113*, 18191-18203.
67. Fu, H.; Duan, Z. Y.; Henkelman, G. Computational Study of Structure and Reactivity of Oligomeric Vanadia Clusters Supported on Anatase and Rutile TiO_2 Surfaces. *J. Phys. Chem. C* **2015,** *119*, 15160-15167.
68. Mullins, D. R.; Radulovic, P. V.; Overbury, S. H. Ordered Cerium Oxide Thin Films Grown on Ru(0001) and Ni(111). *Surf. Sci.* **1999,** *429*, 186-198.
69. Matolin, V.; Libra, J.; Matolinova, I.; Nehasil, V.; Sedlacek, L.; Sutara, F. Growth of Ultra-Thin Cerium Oxide Layers on Cu(111). *Appl. Surf. Sci.* **2007,** *254*, 153-155.
70. Duchon, T.; Dvorak, F.; Aulicka, M.; Stetsovych, V.; Vorokhta, M.; Mazur, D.; Veltruska, K.; Skala, T.; Myslivecek, J.; Matolinova, I., et al. Ordered Phases of Reduced Ceria as Epitaxial Films on Cu(111). *J. Phys. Chem. C* **2014,** *118*, 357-365.
71. Fronzi, M.; Soon, A.; Delley, B.; Traversa, E.; Stampfl, C. Stability and Morphology of Cerium Oxide Surfaces in an Oxidizing Environment: A First-Principles Investigation. *J. Chem. Phys.* **2009,** *131*, 104710.
72. Zavalij, P. Y.; Whittingham, M. S. Structural Chemistry of Vanadium Oxides with Open Frameworks. *Acta Crystallogr. B* **1999,** *55*, 627-663.
73. Ganduglia-Pirovano, M. V.; Sauer, J. Stability of Reduced V_2O_5(001) Surfaces. *Phys. Rev. B* **2004,** *70*, 045422.
74. Martinez-Huerta, M. V.; Coronado, J. M.; Fernandez-Garcia, M.; Iglesias-Juez, A.; Deo, G.; Fierro, J. L. G.; Bañares, M. A. Nature of the Vanadia-Ceria Interface in V^{5+}/CeO_2 Catalysts and Its Relevance for the Solid-State Reaction toward $CeVO_4$ and Catalytic Properties. *J. Catal.* **2004,** *225*, 240-248.
75. Da Silva, J. L. F.; Ganduglia-Pirovano, M. V.; Sauer, J. Formation of Cerium Orthovanadate ($CeVO_4$): A DFT+U Study. *Phys. Rev. B* **2007,** *76*, 125117.
76. Reidy, R. F.; Swider, K. E. Determination of the Cerium Oxidation-State in Cerium Vanadate. *J. Am. Ceram. Soc.* **1995,** *78*, 1121-1122.
77. Abu Haija, M.; Guimond, S.; Romanyshyn, Y.; Uhl, A.; Kuhlenbeck, H.; Todorova, T. K.; Ganduglia-Pirovano, M. V.; Döbler, J.; Sauer, J.; Freund, H. J. Low Temperature Adsorption of Oxygen on Reduced V_2O_3(0001) Surfaces. *Surf. Sci.* **2006,** *600*, 1497-1503.

TOC Graphic: